Smart Materials and Structures

A smart multi-functional printed sensor for monitoring curing and damage of composite repair patch

A smart multi-functional printed sensor for monitoring curing and damage of composite repair patch

Dimitrios G Bekas*, Zahra Sharif-Khodaei, Ferri M H Aliabadi

Structural integrity and Health Monitoring group, Department of Aeronautics, Imperial College London, South Kensington Campus, Exhibition Road, SW7 2AZ London, UK

*Corresponding author: d.bekas@imperial.ac.uk, z.sharif-khodaei@imperial.ac.uk, m.h.aliabadi@imperial.ac.uk

Abstract

A novel multifunctional diagnostic sensor is developed as a cost-effective, in-service structural health monitoring (SHM) system for determining the initial quality of curing of a bonded composite repair patch and assessing its long-term durability on composite structure. The proposed multi-functional sensor technology involves the creation of a "tailor-to-order" 2D conductive patterns onto step-sanded repair surface of composite repair patch using inkjet printing. In employing this methodology, bondline quality during curing and in service was successfully assessed via impedance spectroscopy and resistance change measurements, respectively. The ability of this technology to effectively monitor the integrity of the bondline and the extent of damage in real-time was investigated by subjecting the scarf-repaired CFRP panels to 3-point bending fatigue and low-velocity impact tests. The obtained results were compared with those of transient infrared thermography (IrT) and ultrasound inspection techniques, thus validating the proposed method.

Keywords: structural health monitoring, cure monitoring, interdigital sensor, composite patch repair, inkjet printing

1 Introduction

Composites have permeated primarily aircraft structures such as wing and fuselage components (A350, B787). Aircraft engineers have to consider the repairability of structural composite components, the quality of the repair, compaction of the repair patch and integrity of the bondline in adhesively bonded repairs. Although adhesively bonded joints have been employed for the repair of secondary structures, the absence of a reliable non-destructive testing (NDT) method for detecting poor bond limits their application to primary structures[1].

Manual repairs are time-consuming, labour intensive and suffer from the lack of consistency due to human error. These difficulties have given rise in the past decade to development of several automated repair technologies [2, 3]. Common issues to all automated systems are the non-destructive inspection and evaluation of damage and verification of the quality of the completed repair. Because the bondline between a patch and a repaired surface is so important to the integrity of the repaired structure, there has been much work in the development of NDI techniques. Existing traditional non-destructive inspection (NDI) techniques utilize a variety of methods such as digital image correlation (DIC) [4, 5] , infrared thermography (IrT) [6], Eddy currents [7-9], ultrasonic testing [10-12] and electrical-based methodologies [13, 14]. More recently, to overcome some of the drawbacks of the NDI techniques such as high expense, long down-time of the structure and required access to the part, structural health monitoring (SHM) techniques have been developed for monitoring the integrity of composite parts. There are a variety of SHM techniques such as those that use Lamb waves [15-20], optical fibers [21-24], electrochemical [25] or resistance [26] sensors. An example of the application of an electrical-based methodology to the structural integrity assessment of adhesively bonded or repaired composites is Kang et. al, [27] where crack initiation and propagation were successfully detected in single lap joints with carbon nanotubes (CNTs) dispersed into the adhesive layer. Damage detection was achieved by measuring the variation of equivalent electrical resistance and capacitance of the bondline. In a recent study, Augustin et al. [28] monitored the structural integrity of scarfed carbon fiber reinforced polymer (CFRP) joints under cyclic loading via electrical resistance measurements by employing a carbon CNT-modified adhesive film. The resistance measurements were recorded via inkjet-printed tracks developed at the bondline and the changes were linked to crack initiation and propagation phenomena. Although these approaches are quite promising for monitoring the structural integrity of a bondline, their employment requires the electrical modification of the adhesive layer [27-29] and/or access to both sides of the composite structure [30]. Each of these NDI techniques require significant amount of equipment and expertise and so far, none have proven completely successful for bondline assessment without either requiring access to both sides of the part or modifying the adhesive layer or using numerus sensors that increase the overall weight of the structure. Therefore, there is a need for an accurate inspection technique which can verify the quality of the bondline at the time of application as well as monitoring its integrity during the service-life of the structure.

SHM has proven to be successful for detecting barely visible impact damage (BVID) in composite parts [31, 32]. Application of SHM for monitoring damage in bondlines has been rather few [33-35]. However, there are no current SHM inspection techniques which can assess the initial quality of the adhesive bond as well as its possible degradation due to impact or fatigue.

In this paper, the development of multi-functional sensors for monitoring the curing and service damage of bonded scarf repair patch with minimum disturbance to the structure and the bondline is presented for the first time. The proposed sensor technology is simple, yet reliable. The multi-functional sensor is designed with a special pattern, consisting of conductive circuits and interdigital sensors, to cover different depths of the scarf repaired composite patch. It is inkjet-printed onto the surface of the scarf-repaired area to monitor (i) the curing process of the adhesive film during repair and (ii) the structural integrity of the bondline during service. The curing of the repair patch is conducted using impedance spectroscopy (IS). The ability of the proposed smart sensor to detect the initiation and propagation of damage within the bondline is investigated by subjecting the scarf-repaired CFRP panels to 3-point bending fatigue and low-velocity impact tests. The result obtained using the proposed SMART sensing technology for a composite patch repair, is compared with the Transient infrared Thermography (IrT) and ultrasound inspection techniques.

2 Multi-functional Smart Sensor for Composite Repair

The proposed multi-functional sensor technology is based on additive manufacturing of conductive circuits onto the bondline of a scarf repair. The novelty of the smart sensor is that it does not change the composition of the adhesive, add extra weight to the structures, or require additional wiring to be permanently installed in or around the bondline. It only requires connection to the printed terminals at the time of interrogation. The printed sensing system is designed to serve two functions: monitoring of the curing process and integrity check during the service life [36]. Depending on the geometry and the number of the scarfs in the repair, the multi-functional smart sensor will be designed to cover the repair patch.

Error! Reference source not found. depicts an example of the proposed multi-functional smart sensor with a designed pattern that consists of five inkjet-printed silver-based circuits and four interdigital sensors.

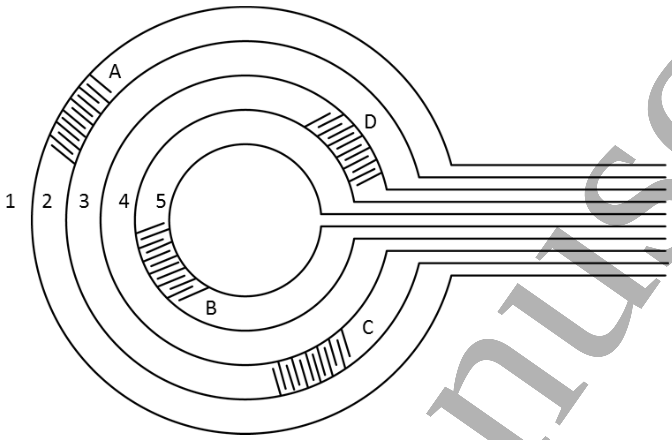

Figure 1 Example of the proposed Multi-functional smart sensor

Figure 2 illustrates the basic concepts for the quality assessment (interdigital sensors) and damage detection (conductive tracks) of the scarf repair using the proposed methodology. The sensors are comprised of an interlocking comb-shaped array of silver electrodes and is used to monitor the progress of cure of the adhesive layer using impedance spectroscopy (IS). For the initiation and propagation of damage within the structure, the disruptions in the conductive circuits are used as indication of a damage event that is located in the bondline.

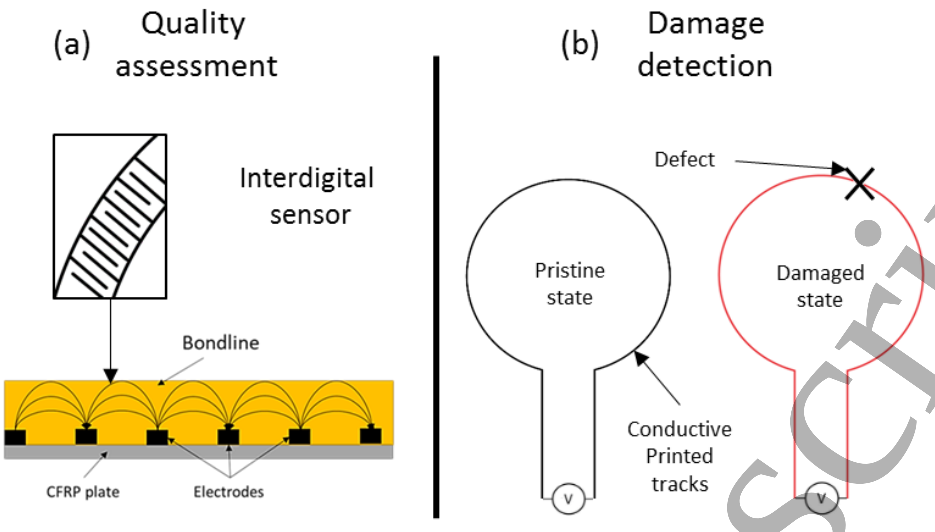

Figure 2 Proposed methods for quality assessment (a) and damage detection (b) using the multi-functional sensor

It should be noted that the circuits can be modified (i.e. shape, number and location) according to the dimensions of the repair and the permissible size of the defect. The development, functionalities and diagnostic methodologies of the proposed smart sensor is detailed in the following sections.

2.1 Development of the Printed Multi-Functional Sensors

For the inkjet printing of the conductive circuits, a silver nanoparticle suspension was employed. The concentration of the nanoparticles was 30-35 wt. %, and their diameter was under 50 nm. The viscosity ranged from 10 to 18mPa·s and the surface tension was between 35 and 40 $mN \cdot m^{-1}$. The printing of the conductive circuits was performed using a piezoelectric Inkjet printer. The piezo voltage was selected at 20 V and the jetting frequency was set at 5kHz. The substrate temperature was selected at 60 °C and the drop spacing was 40 µm. The width of the printed tracks was set at 1 mm. To enhance the electrical conductivity of the printed circuits, 5 layers of silver-based ink were printed on top of each other. It should be noted that no sintering process, for the silver-based tracks, was necessary since the repair process occurred at elevated temperatures which resulted in sintering of the silver ink, the removal of the remaining traces of solvents and the fusion of the conductive particles into a cohesive conductive track.

To characterize the quality of the printed process, the electrical resistance of the inkjet-printed circuits was measured via the 4-probe method, using a multimeter. The electrical resistivity is then calculated using:

$$\rho = R * \frac{A}{l} \tag{1}$$

where R is the resistance, l and A are the length and the cross-sectional area of the wire, respectively. The resistivity of the printed circuits was calculated to be 10 μΩ cm which is slightly lower than that reported in the ink datasheet.

2.2 Cure Monitoring

To access the quality of the bondline, the curing of repair process is monitored with the printed interdigital sensors using Impedance Spectroscopy. Impedance spectroscopy is a technique that can be employed in order to investigate the processing characteristics, chemical structure or structural integrity of polymers and their composite materials by measuring their impedance properties [37-43]. Impedance measurements involve the application of a monochromatic voltage to the material while the resulting current is measured at that frequency. A spectrum is generated by sweeping in a range of frequencies and measuring the impedance at each point. It is only necessary for the interdigital sensors to have access to one side of the material, as the signal's penetration depth can be controlled by modifying the sensor area, the number of fingers, and the spacing between them [44]. In general, when a material interacts with an external electric field, ions that are present in the material start to move towards the electrode of opposite polarity, while dipoles try to align with the external electric field. The mobility of these charged species is highly affected by the phase transitions in the material (i.e. curing of an epoxy). A quantity that can be directly related to the mobility of the charged species within the material is the maximum of imaginary part of the impedance (Z''_{max})[37]. Therefore, this parameter is chosen for monitoring the curing process for the proposed multi-functional sensor technology.

2.3 Integrity Monitoring of Repair Patch

The printed conductive circuits are also designed for monitoring the integrity of the repair patch. Each circuit is printed at different depth of the scarf repair. The principle of the integrity monitoring is that as long as the circuits are intact, the terminals of the conductive circuits will have a consistence resistivity. Once damage will be present in the bondline, the connection will be lost, thus no resistance will be outputted.

3 Application of Multi-Functional Smart sensor to Composite Patch Repair

In order to asses and validate the developed methodologies and technologies, the multi-functional sensor was applied to a bonded repair patch. A 16-ply specimen (Hexply 914-TS-5-134 prepreg) with $[0/+45/-45/90]_{2s}$ stacking sequence and 250mm x 250mm x 2mm dimensions was manufactured. The plate was manually scarfed to the required scarf angle and depth using a Leslie Composite Repair kit. Three plies of carbon fibers were completely removed. Afterwards, a thin layer of epoxy resin, Prime 20 LV, was screen coated onto the scarfed surface of the panels to electrically isolate the printed tracks from the carbon fibers.

The step-sanded repair was made using 4 Hexply 914 plies with an overlap length of 15mm and a 914 epoxy film. A polytetrafluoroethylene (PTFE) tape with dimensions of 14mm x 18mm was inserted at the edge of the repair patch to initiate a crack propagation in the bondline during the mechanical testing. The repair process occurred in a purposely developed mold that was placed in a laboratory oven under the pressure of 1 bar. Curing took place 2 steps: (i) heating up to 175 ^{0}C at a rate of 6^{0}C/min and (ii) 60 min at 175^{0}C. The three steps of the experimental process for the development of the conductive pattern on the scarf repaired CFRP panels are illustrated in Figure 3.

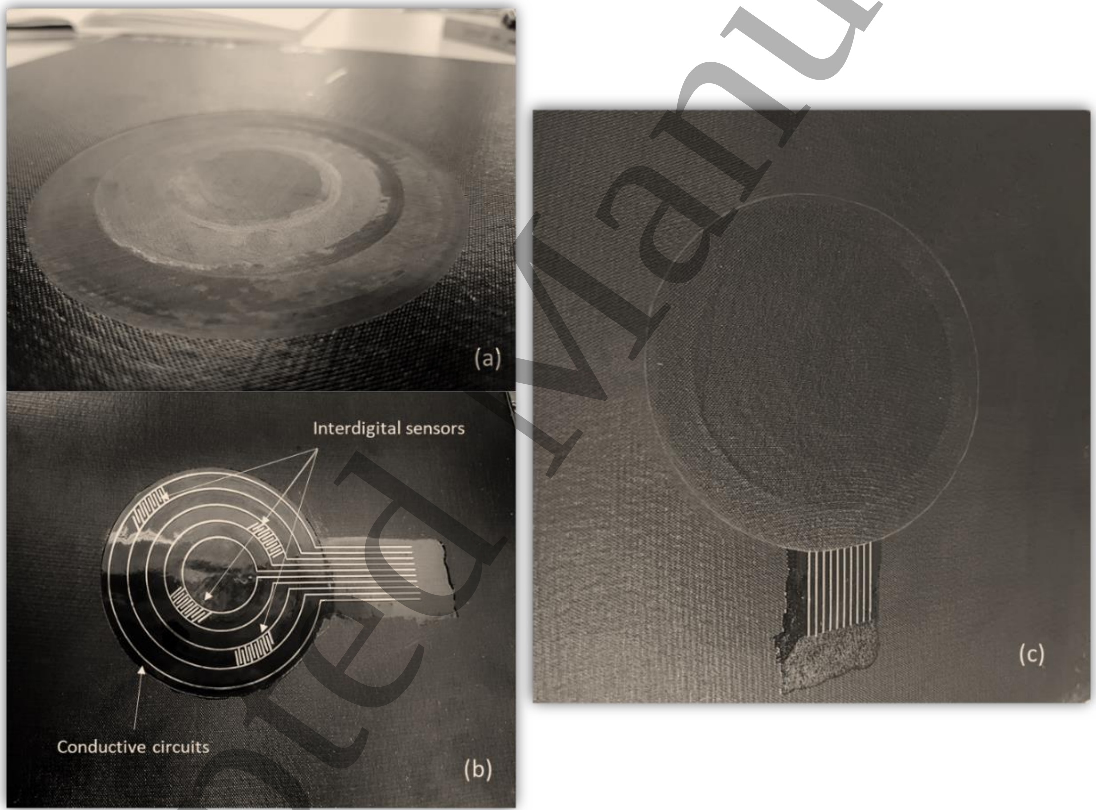

Figure 3 (a) Ply removal, (b) printing of the conductive pattern and (c) final scarf repaired CFRP panel

3.1 Cure Monitoring of Bonded Patch Repair

For monitoring the curing of the repair patch, four interdigital sensors were inkjet-printed onto the scarfed surface of the panels at different depths. To examine the ability of the developed sensors to detect a defect at the bondline during manufacture, a small piece of epoxy film at the location of sensor D was replaced by a Kapton film to simulate a defect in the bondline. A sinusoidal electrical excitation waveform of varying frequency was applied by the spectrometers, and the induced current waveform was recorded. The excitation frequency ranged from 20 Hz to 3 MHz, while the voltage amplitude was set at 1 V. The temperature of the specimen during the repair process was monitored with a thermocouple.

The maximum of the imaginary part of the impedance (Z''_{max}) is affected by the phase transitions in the material; therefore, it is a good indicator for monitoring the quality of the curing of the epoxy. Figure 4 depicts the evolution of Z''_{max} during the repair process for the four developed sensors.

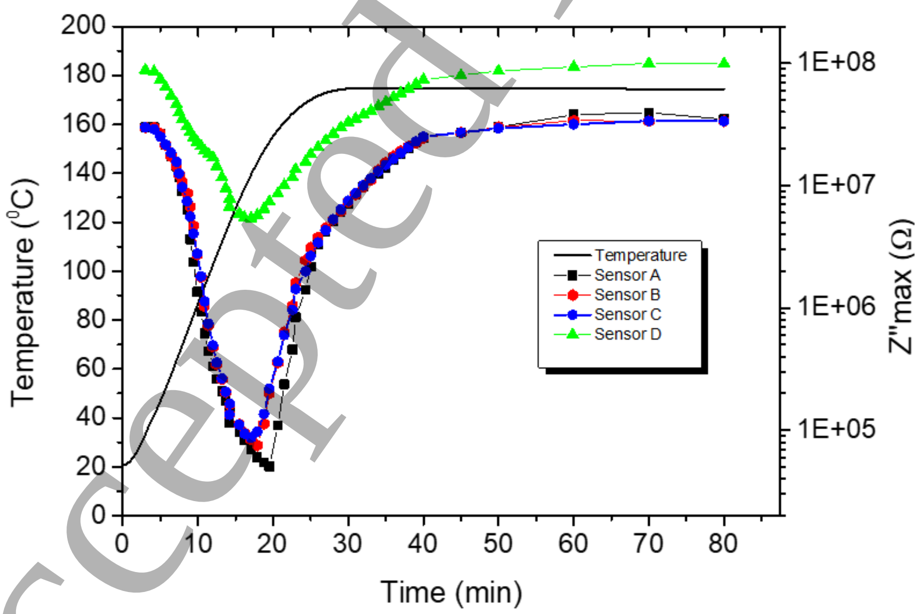

Figure 4 The evolution of the maximum of the imaginary part of the impedance (Z''_{max}) during the repair process for the four developed sensors

As can be observed, the Z''_{max} curves of the sensors A, B and C are almost identical. However, sensor D shows significantly different behavior, indicating the presence of a defect that was created during the repair process. The Z''_{max} curves can be divided into three main regions that represent different states of the bonding process. At the beginning where the epoxy film was still in the solid state, the Z''_{max} values of the sensors A, B and C were recorded at $3x10^7$ Ω. As the temperature increased, the viscosity of the system is considerably reduced, and the epoxy film transited from a solid to a liquid phase. This resulted in a significant increase in ionic mobility, manifested as an abrupt decrease in the Z''_{max} values by approximately two orders of magnitude. After 20 min, the Z''_{max} values reached a minimum value of $5x10^5$ Ω, indicating the initiation of the reaction [37, 40]. In the second stage of the bonding process, the Z''_{max} values experienced an initial rapid increase, which was associated with the gelation of the epoxy film, followed by a slower rate of increase. At the final stage of the repair process, the Z''_{max} values stabilized, indicating the complete cure of the epoxy film.

3.2 Bondline Integrity of Bonded Patch Repair

To assess the proposed smart patch technology under operational conditions, two identical specimens were manufactured and subjected to two mechanical tests simulating the service life conditions: fatigue and low velocity impact tests were selected to induce barely visible damage in the bondline. To validate the proposed sensing technology for application to composite patch repair, the obtained results were compared with infrared thermography (IrT) and ultrasound inspection techniques. An IR camera was used for the NDE of the repaired CFRP panels. The camera is capable of acquiring full-frame 16-bit images at a frame rate of 50 Hz. An Ir-lamp was used as a heat source. The recording duration of the IR camera was 30 s to monitor an entire period of heating and cooling. In the case of impact testing, the damaged area was also investigated using ultrasound inspection.

3.2.1 Fatigue testing

The selected cyclic frequency was f = 1 Hz, the maximum displacement was 8 mm and the stress ratio was R = 0.2. To assess the structural integrity of the bondline in real time, electrical resistance measurements were conducted during the testing using two digital Multimeters. Figure 5a) depicts the 3-point fatigue bending test while Figure 5b and c show a top and side view illustrations of the scarf repaired panel, respectively.

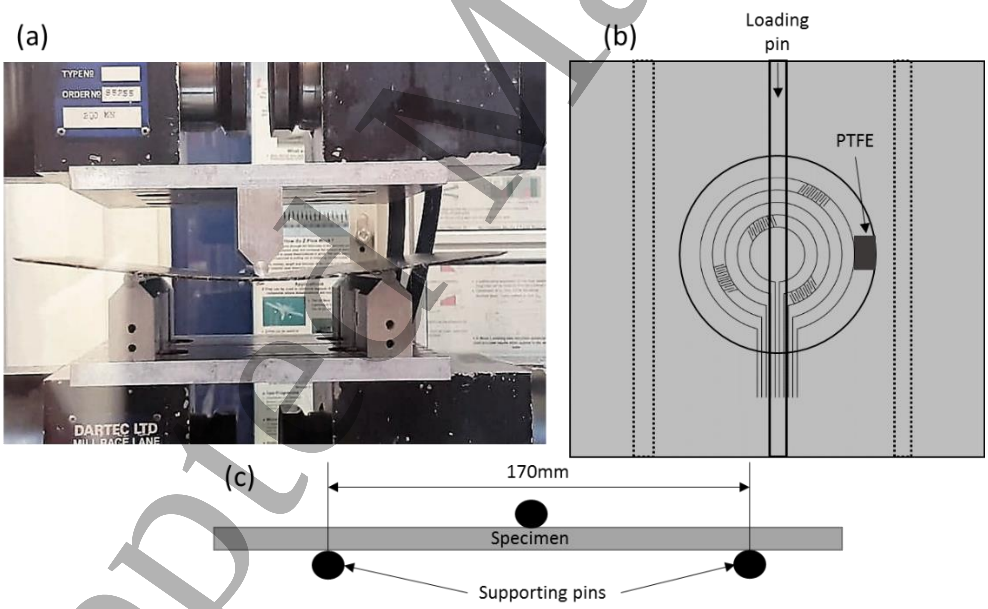

Figure 5 (a) 3-point fatigue bending test, (b) top and (c) side view of the scarf repaired panel

The integrity of the bondline was monitored in real-time by tracking the change in the resistance of the inkjet-printed circuits. Upon damage, the conductive circuits were interrupted and the connections between the two terminals of the multimeter were lost (Figure 2b). At that moment, the fatigue testing was stopped, and the integrity of the repair was investigated using Ir-thermography. Figure 6 depicts the resistance values of the five printed circuits at different fatigue loading cycles.

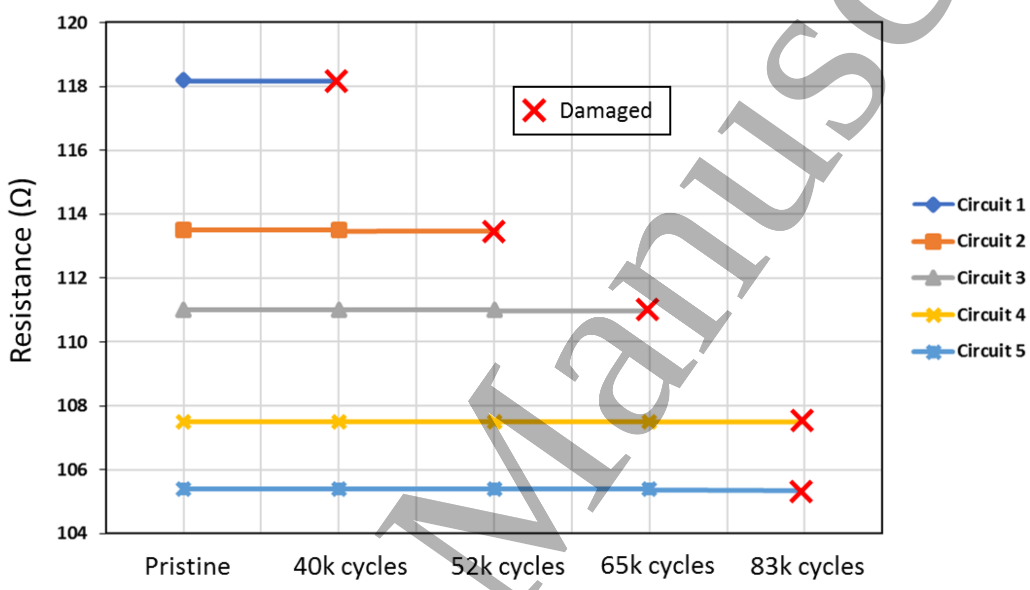

Figure 6 Electrical resistance values of the five conductive sensors at different fatigue cycles.

For the pristine repaired CFRP plate, all five circuits remained intact and the resistance values ranged between 105-120Ω. After 40k fatigue cycles, the connections between the terminals of circuit 1 were lost, indicating the presence of damage in the bondline close the edge of the repair patch. At the same time, the connection between the remaining four circuits remained intact and their resistance remained unchanged. Whenever a connection was lost, the plate was removed from the fatigue machine and the integrity of the patch repair was investigated via Ir-T, and the fatigue test was continued under the same loading conditions. Testing stopped another two times, when the connections of circuits 2 and 3 were lost after 52k and 65k fatigue cycles respectively. This indicates that the damage propagated in the bondline between the patch and the repaired panel. The same approach was followed until the connection of all circuits were lost. This occurred after 83k fatigue cycles. An important advantage of this methodology is that since the detection of damage is restricted to the blond-line, it is not affected by any degradation of the repair patch or of the composite panel.

To validate the sensor response, IR thermography is used to assess the damage to the bondline. The thermographs obtained from the scarf-repaired panel at different fatigue cycles are depicted in Figure 7 and the induced damage is highlighted with red dashed lines.

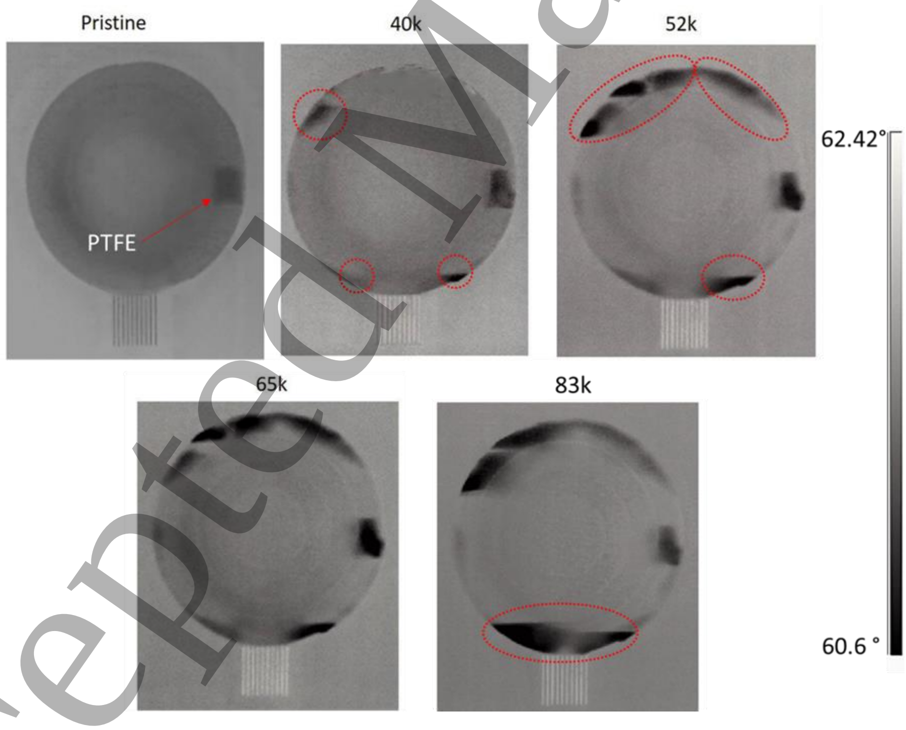

Figure 7 Thermographs obtained from the scarf-repaired panel at different fatigue cycles

266 After 40k cycles, the initiation of the detachment between the patch and the panel did not occur at the location of the PTFE. This can be attributed to the increased stress concentrations in areas located near the support from where load was applied (Figure 5). After 52k fatigue cycles, the damage propagated towards the center of the repair patch and the perimeter of the overlap layer. At this point, the connection of circuit 2 was lost while the rest of the circuits remained intact. The results obtained from the third thermograph after 65k fatigue cycles suggests that the damage propagated at the perimeter of the patch, destroying the connections of circuit 3. All circuit connections were lost after 83k fatigue cycles when the propagating crack completely destroyed the silver tracks located at the perimeter of the overlapping layer.

3.2.2 Low velocity impact testing

A drop tower was used to impact the CFRP panel on the edge of the scarf repair where the PTFE film was located to weaken the bond. This location was selected to ensure that the induced damage will be in the bondline between the plate and the composite. A hemispherical impactor with a radius of 20 mm and a mass of 2.41 kg was used. The impact testing was conducted at ambient conditions with temperature and relative humidity of 23 ^{0}C and 50-60%, respectively. The impact energy was set at 8J, simulating the events of a tool drop or bird impact. At the end of the impact testing, electrical resistance measurements were conducted in order to evaluate the extent of damage within the bondline. IrT and ultrasound inspection techniques were also employed to evaluate the bondline integrity to validate the proposed sensor technology. At the end of the impact testing, electrical resistance measurements were taken from the silver-based circuits using a 72 Pro IDM71 Digital Multimeter by RS. The drop tower, along with the scarf repaired CFRP panel, is depicted in Figure 8.

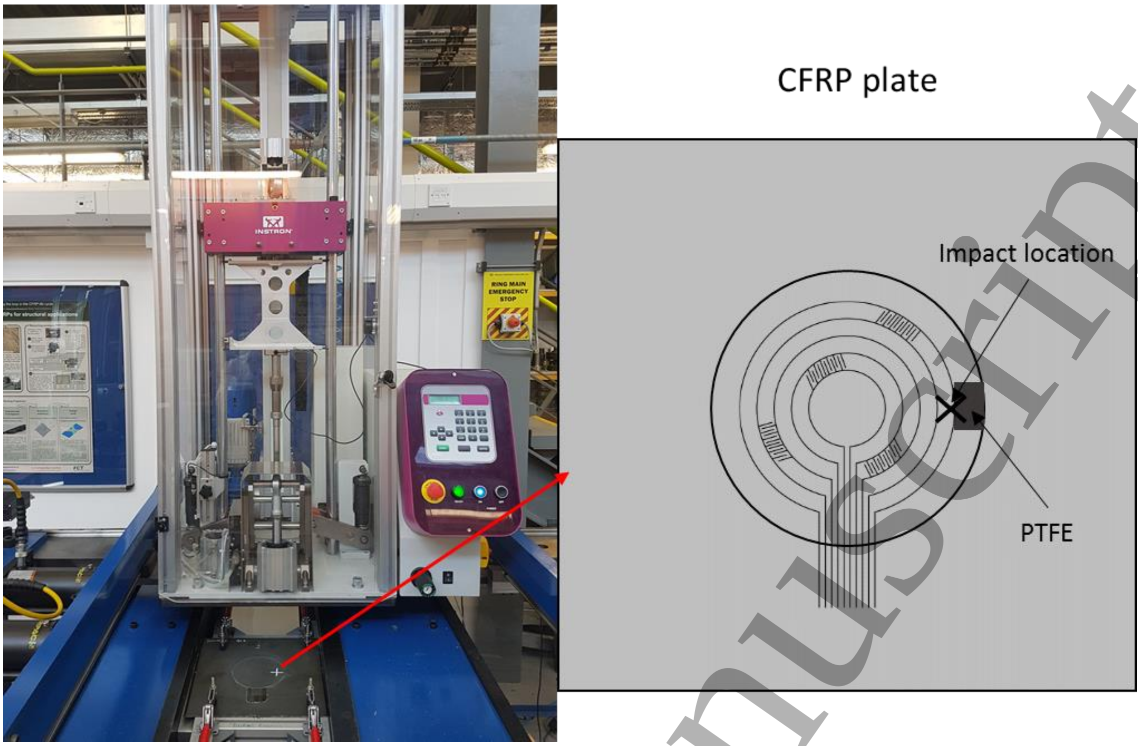

Figure 8 The Instron CEAST 9350 drop tower used for impacting(left), and the composite panel and location of impact (right)

The electrical resistance values of the five conductive circuits before and after the impact testing are summarized in the bar chart in Figure 9.

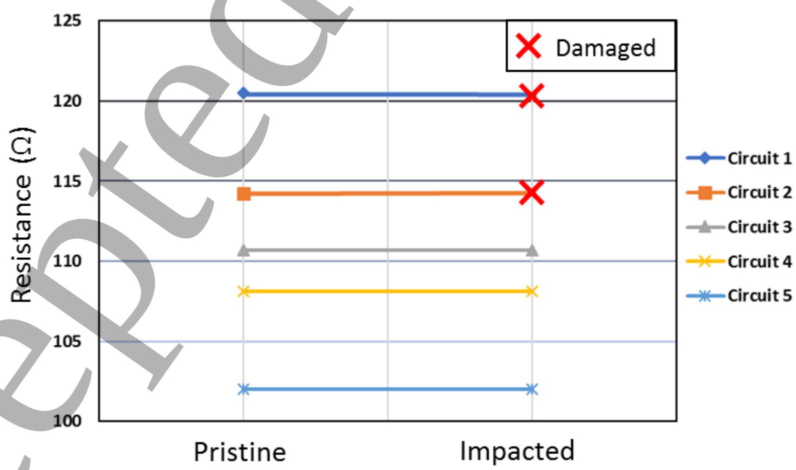

Figure 9 Electrical resistance values of the conductive circuits before and after the impact testing

As expected, when a circuit was “lost” its resistance could not be measured, indicating the presence of damage in the bondline within the radius of the circuit. As can be observed, the induced damage resulted in the disruption of 2 conductive silver-based circuits while the rest of the circuits remained intact. Electrical measurements indicated that the integrity of the two exterior circuit was damaged. Thus, the extent of the damage within the bondline was approximately 10 mm from the PTFE film.

Figure 10(a) depicts the thermographs obtained from the pristine (undamaged) and the impacted CFRP panel during the cooldown process. A graphical representation of the conductive circuits (without the interdigital sensors) is shown in Figure 10(b).

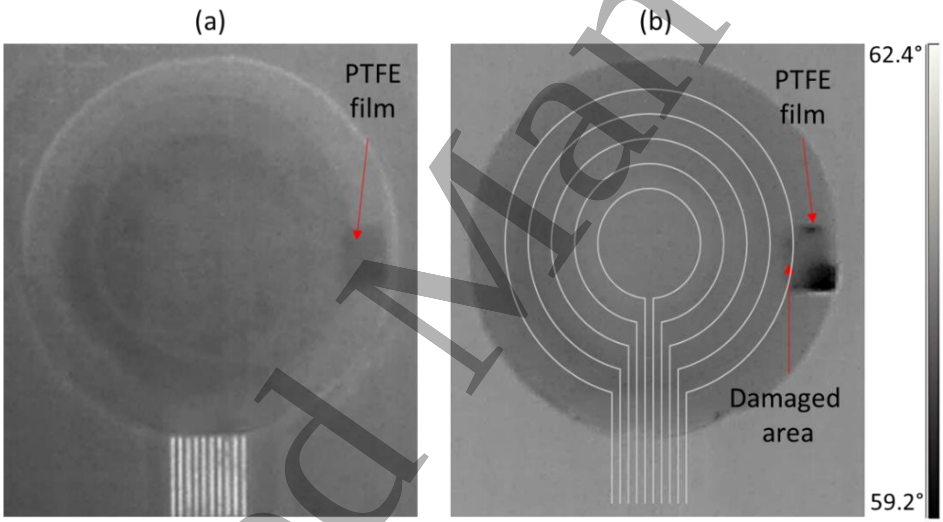

Figure 10 Thermographs obtained from the scarfed repaired panels (a) before and (b) after the impact testing

In the thermograph of the pristine repaired CFRP plate, the artificially created defect (PTFE) in the patch between the plate and adhesive layer was readily revealed by infrared thermography. As can be observed in Figure 10(b), the induced impact damage to the bondline affected the two exterior conductive circuits that were printed onto the repaired area.

To further examine the extent of the damage created by the impact test, the damaged area was examined using ultrasound inspection. Figure 11(b) and (c) depict the C-scan images obtained from the pristine and damaged CFRP panels, respectively.

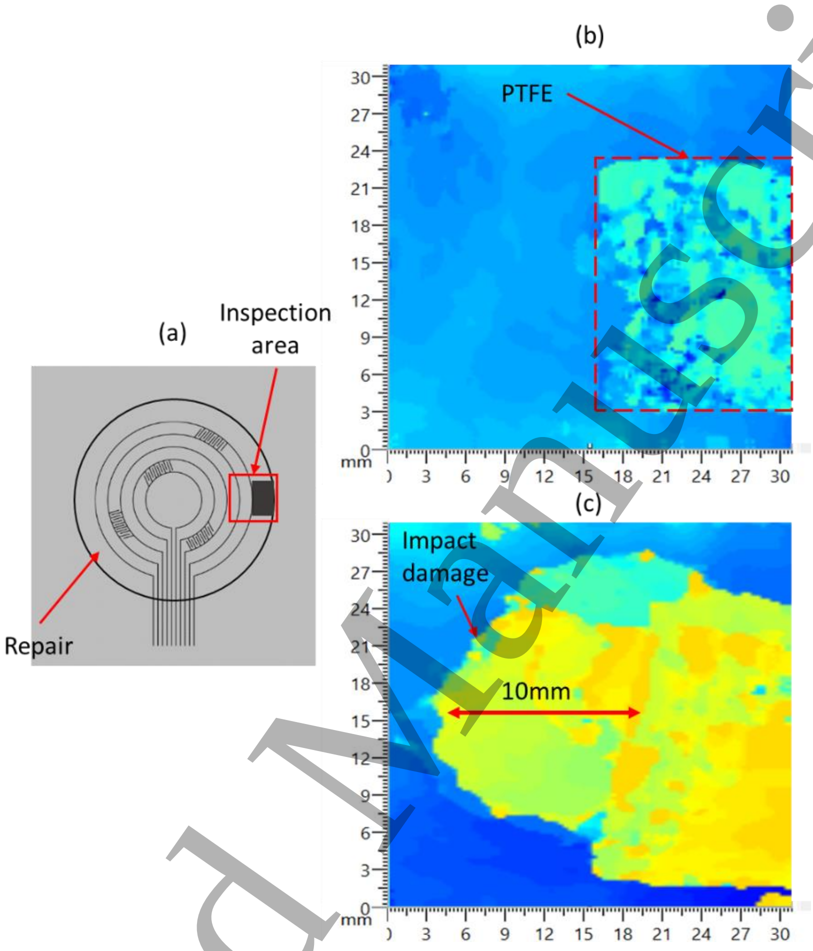

Figure 11 (a) Inspection area; C- scan images obtained from the (b) pristine and (c) damaged CFRP panel

The artificially created defect can be seen in Figure 11 (a). After the impact test, the damaged area increased at about 10 mm towards the center of the repair. It should be mentioned that the yellow color shows increased severity (Figure 11(b)). The C-scan images show that the damage propagated at approximately 10 mm from its initial position towards the center of the repair. This observation is in agreement with the results obtained from the resistance measurements which suggested that the two exterior circuits were disrupted due to the induced damage.

4 Conclusions

In the present work, a novel multi-functional sensor for the quality assessment and structural health monitoring of a bonded composite repair was successfully developed and tested. The proposed smart repair technology is reliable and has minimum interference with the functionality of the bonded repair patch, i.e. no additional weight, no additional wiring and no chemical changes to the composition of the epoxy. The multi-functional sensor system consisted of inkjet-printed silver-based circuits and interdigital sensors. The architecture of the smart repair patch can be tailored to the repaired area and the repair technique as well as the minimum size of the defect to be detected.

The functionality of the proposed smart patch was tested for cure monitoring and integrity assessment of the bondline with proposed test campaign. The bondline quality assessment during the cure monitoring was evaluated through impedance spectroscopy measurements. Results indicate that the developed sensors were able to successfully identify defects in the bondline during the repair process by tracing the evolution of the maximum value of the impedance imaginary component.

Concerning the SHM of the repair, the repaired CFPR plates were subjected to 3-point bending fatigue and low-velocity impact tests to cause barely visible damage in the bondline. Electrical resistance measurements were recorded from the printed circuits, providing real-time information regarding the structural integrity of the bondline. The proposed concept was based on a simple but effective assumption; any induced damage within the bondline will result in a discontinuity of the conductive circuits that would be manifested by the lost connections between their terminals. In the case of fatigue testing, the proposed methodology was able to detect damage initiation and propagation within the bondline by identifying lost connections caused by the disruption of the conductive circuits at different fatigue cycles. The developed patch was also capable of identifying damage caused by a low-velocity impact, with the induced damage disrupting the conductive circuits. In both test cases, the methodology was validated by comparing the results obtained from electrical resistance measurements with infrared thermography and ultrasound inspection techniques.

5 Declaration

The authors would like to declare that there is a pending patent regarding the multi-functional sensor. The patent application number is GB1906841.0.

6 References

1. S. Pavlopoulou, K. Worden and C. Soutis, Journal of Intelligent Material Systems and Structures **27** (4), 549-566 (2015).
2. A. Baldan, JOURNAL OF MATERIALS SCIENCE **39**, 1– 49 (2004).
3. K. B. Katnam, L. F. M. Da Silva and T. M. Young, Progress in Aerospace Sciences **61**, 26-42 (2013).
4. M. A. Caminero, S. Pavlopoulou, M. Lopez-Pedrosa, B. G. Nicolaisson, C. Pinna and C. Soutis, Composite Structures **95**, 500-517 (2013).
5. L. Toubal, M. Karama and B. Lorrain, Composite Structures **68** (1), 31-36 (2005).
6. (!!! INVALID CITATION !!! 6-8).
7. H. Heuer, M. Schulze, M. Pooch, S. Gäbler, A. Nocke, G. Bardl, C. Cherif, M. Klein, R. Kupke, R. Vetter, F. Lenz, M. Kliem, C. Bülow, J. Goyvaerts, T. Mayer and S. Petrenz, Composites Part B: Engineering **77**, 494-501 (2015).
8. Y. He, G. Tian, M. Pan and D. Chen, Composites Part B: Engineering **59**, 196-203 (2014).
9. R. R. Hughes, B. W. Drinkwater and R. A. Smith, Composites Part B: Engineering **148**, 252-259 (2018).
10. D. G. Aggelis, N. M. Barkoula, T. E. Matikas and A. S. Paipetis, Composites Science and Technology **72** (10), 1127-1133 (2012).
11. J. Dong, B. Kim, A. Locquet, P. McKeon, N. Declercq and D. S. Citrin, Composites Part B: Engineering **79**, 667-675 (2015).
12. D. Palumbo, R. Tamborrino, U. Galietti, P. Aversa, A. Tatì and V. A. M. Luprano, NDT & E International **78**, 1-9 (2016).
13. A. Vavouliotis, A. Paipetis and V. Kostopoulos, Composites Science and Technology **71** (5), 630-642 (2011).

14. M. Morozov, W. Jackson and S. G. Pierce, Composites Part B: Engineering **113**, 65-71 (2017).
15. F. Lambinet, Z. Sharif Khodaei and M. H. Aliabadi, Key Engineering Materials **713**, 135-138 (2016).
16. F. Lambinet, Z. Sharif Khodaei and M. Aliabadi, H. , Key Engineering Materials (2017).
17. Z. Sharif-Khodaei and M. H. Aliabadi, Smart Materials and Structures **23** (7) (2014).
18. S. Pavlopoulou, S. A. Grammatikos, E. Z. Kordatos, K. Worden, A. S. Paipetis, T. E. Matikas and C. Soutis, Composite Structures **127**, 231-244 (2015).
19. J.-B. Ihn and F.-K. Chang, Smart Materials and Structures **13** (3), 621-630 (2004).
20. H. Fu, Z. S. Khodaei and M. H. F. Aliabadi, IEEE Internet of Things Journal, 1-1 (2018).
21. A. R. Wilson, C. Davis, W. Baker, S. D. Moss, S. C. Galea and R. Jones, in *Smart Materials II* (2002).
22. W. Baker, I. McKenzie and R. Jones, Composite Structures **66** (1-4), 133-143 (2004).
23. I. McKenzie, R. Jones, I. H. Marshall and S. Galea, Composite Structures **50**, 405-416 (2000).
24. R. Jones and S. Galea, Composite Structures **58**, 397–403 (2002).
25. G. D. Davis, K. Thayer, M. J. Rich and L. T. Drzal, Journal of Adhesion Science and Technology **16** (10), 1307-1326 (2002).
26. S. A. Grammatikos, E. Z. Kordatos, T. E. Matikas and A. S. Paipetis, Journal of Materials Engineering and Performance **23** (1), 169-180 (2013).
27. M.-H. Kang, J.-H. Choi and J.-H. Kweon, Composite Structures **108**, 417-422 (2014).
28. T. Augustin, J. Karsten, B. Kötter and B. Fiedler, Composites Part A: Applied Science and Manufacturing **105**, 150-155 (2018).
29. R. Mactabi, I. D. Rosca and S. V. Hoa, Composites Science and Technology **78**, 1-9 (2013).
30. A. S. Lim, Z. R. Melrose, E. T. Thostenson and T.-W. Chou, Composites Science and Technology **71** (9), 1183-1189 (2011).
31. M. S. Salmanpour, Z. Sharif Khodaei and M. H. F. Aliabadi, Sensors (Basel) **17** (5) (2017).
32. X. Zhao, H. Gao, G. Zhang, B. Ayhan, F. Yan, C. Kwan and J. L. Rose, Smart Materials and Structures **16** (4), 1208-1217 (2007).
33. S. Takeda, T. Yamamoto, Y. Okabe and N. Takeda, Smart Materials and Structures **16** (3), 763-770 (2007).
34. X. Yu, Z. Fan, S. Puliyakote and M. Castaings, Smart Materials and Structures **27** (3) (2018).
35. F. Lambinet, Z. Sharif Khodaei and F. M. H. Aliabadi, Key Engineering Materials **774**, 535-540 (2018).
36. D. G. Bekas, Z. Sharif Khodaei and F. M. H. Aliabadi, Key Engineering Materials **774**, 235-240 (2018).
37. A. A. SKORDOS and K. P. IVANA, Journal of Polymer Science Part B: Polymer Physics **42**, 146-154.

38. D. G. Bekas, G. Gkikas, G. M. Maistros and A. S. Paipetis, RSC Advances **6** (82), 78838-78845 (2016).

39. D. G. Bekas and A. S. Paipetis, Composites Science and Technology **134**, 96-105 (2016).

40. K. Kalkanis, G. J. Tsamasphyros, G. N. Kanderakis, N. Pantelelis, M. Tur, G. Maistros and Y. Botsev, Sensor Letters **9** (4), 1265-1272 (2011).

41. D. G. Bekas and A. S. Paipetis, Journal of Sensors **2015**, 1-7 (2015).

42. D. Baltzis, D. G. Bekas, G. Tzachristas, A. Parlamas, M. Karabela, N. E. Zafeiropoulos and A. S. Paipetis, Composites Science and Technology **153**, 7-17 (2017).

43. D. G. Bekas, Z. Sharif-Khodaei, D. Baltzis, M. H. F. Aliabadi and A. S. Paipetis, Composite Structures **211**, 557-563 (2019).

44. A. V. Mamishev, K. Sundara-Rajan, Y. Fumin, D. Yanqing and M. Zahn, Proceedings of the IEEE **92** (5), 808-845 (2004).